Materials Science & Engineering C 123 (2021) 111955

Contents lists available at ScienceDirect

Materials Science & Engineering C

journal homepage: www.elsevier.com/locate/msec

Development of collagen/nanohydroxyapatite scaffolds containing plant extract intended for bone regeneration

Claudio Fernandes Garcia [a,*], Crisiane Aparecida Marangon [b], Lívia Contini Massimino [b], Maria Fátima Guarizo Klingbeil [c], Virginia Conceição Amaro Martins [a], Ana Maria de Guzzi Plepis [a,b]

[a] São Carlos Institute of Chemistry (IQSC), University of São Paulo (USP), São Carlos 13560-970, Brazil
[b] Interunits Graduate Program in Bioengineering (EESC/FMRP/IQSC), University of São Paulo (USP), São Carlos 13566-590, Brazil
[c] Nuclear and Energy Research Institute (Ipen), São Paulo 05508-000, Brazil

ARTICLE INFO

Keywords:
Collagen
Nanohydroxyapatite
Flavonoids
Bone regeneration

ABSTRACT

In this study scaffolds of nanohydroxyapatite (nHA) and anionic collagen (C) combined with plant extracts intended for bone tissue repair were developed. Grape seed (P), pomegranate peel (R) and jabuticaba peel (J) extracts were used as collagen crosslinker agents in order to improve the materials properties. All crude extracts were effective against *Staphylococcus aureus*, but only for CR scaffold inhibition zone was noticed. The extracts acted as crosslinking agents, increasing enzymatic resistance and thermal stability of collagen. The extracts showed cytotoxicity at the concentrations tested, while nHA increased cell viability. The scaffolds presented porosity and pore size appropriate for bone growth. CR, CnHAP, CnHAR and CnHAJ increased the cell viability after 24 h. The combination of collagen, nHA and plant extracts offers a promising strategy to design novel biomaterials for bone tissue regeneration.

1. Introduction

Bone tissue is composed by an organic part, mainly type I collagen (C) - a fibrous protein present in the animal kingdom, and an inorganic part, mainly calcium phosphate in hydroxyapatite form (HA) [1]. Moreover, the composition and structure of bone vary with the age, genetic inheritance, and living conditions of patients, resulting in different demands for bone implants [2]. The most common solutions for bone implants are autografts and allografts treatments. However, they have some drawbacks such as the limited sources, extra invasive surgery and immunological rejection.

For these reasons, more attention has been drawn to bone tissue engineering, an attractive strategy that combine biotechnology and biomaterials to mimic the composition of bone tissue, which can replace or repair it. Despite considerable advances in biomaterials-based approaches, the development of ideal materials that fulfill the requirements for bone repair continue to present challenges.

HA-collagen-based materials have emerged as promising candidates to prepare scaffolds and overcome unmet needs in the field of bone tissue engineering. Collagen has properties to stimulate and guide the natural tissue formation. It is responsible for the physical properties of the tissues that form the skin, tendons, intestines, bones, and teeth [3]. Hydroxyapatite is a bioceramic that, like collagen, can stimulate and guide the bone tissue formation. Hydroxyapatite in nanoparticulate form (nHA) is likely to be more bioactive than a micro sized one, allowing better protein sorption and cell adhesion, which accelerates bone repair [4]. In addition, they possess good biocompatibility and bioactivity, as well as controllable biodegradability, being able to induce bone regeneration and reduce the treatment time. Collagen and hydroxyapatite scaffolds can also be modified to improve physicochemical and clinical properties of biomaterials [5]. These alterations can occur by chemical modifications in the collagen itself or by the addition of other polymers/crosslinking agents.

Recent studies have developed novel biomaterials constructs, including scaffolds of collagen and HA, for bone tissue engineering. He et al. [6] developed collagen and HA-based materials with microfibrillated cellulose for bone regeneration and highlighted that the materials obtained had adequate physicochemical properties to be used for this application. Minardi et al. [7] produced type I collagen scaffolds with magnesium doped HA and concluded that the biomaterial has great

* Corresponding author.
E-mail address: claudiofgarcia@alumni.usp.br (C.F. Garcia).

https://doi.org/10.1016/j.msec.2021.111955
Received 17 November 2020; Received in revised form 26 January 2021; Accepted 5 February 2021
Available online 11 February 2021

osteoinductive and osteoconductive capacity, playing a vital role in the bone reconstruction area.

The addition of bioactive compounds such as plant extracts and essential oils to collagen and HA-based materials can be other strategy to improve their properties due to the strong antioxidant, antimicrobial, antifungal, anti-inflammatory, and antiviral capacity [8]. Further the flavonoids can act as collagen crosslinking agents, which can improve the mechanical and thermal resistance of the biopolymer, besides its metabolites protect the polymeric matrix from oxidation. Song et al. [9] developed collagen scaffolds obtained from duck feet, with HA and quercetin, a polyphenolic compound of the flavonoid group. They concluded that the collagen scaffold, HA and 25 μmol^{-1} of quercetin increases cell proliferation and osteogenic differentiation, accelerating bone regeneration.

Among the various phenolic extracts reported in literature, the extracts of grape seed, pomegranate and jabuticaba peel (the latter a Brazilian fruit) stand out as rich flavonoids sources. Although, there are many studies with collagen and hydroxyapatite to formulate a material for bone regeneration, few studies using flavonoids incorporated to anionic collagen and nanohydroxyapatite scaffolds have been done.

Thus, the main objectives of this study are the development of smart scaffolds prepared by anionic collagen [10], nanohydroxyapatite and natural extracts as well as assessing their physicochemical and biological properties. As far as we know, there is no previous study in the literature that addresses this fact and evaluates the effect of fruit extracts addition on the characteristics of the formed scaffolds.

2. Materials and experimental

2.1. Anionic collagen preparation

Collagen was prepared from porcine serous, by alkaline hydrolysis in solution of hydroxides, chlorides, and sulfates of K^+, Ca^{2+} and Na^+ for 120 h. This solution promotes the selective hydrolysis of carboxyamide groups of the collagen, increasing the negative charge of the biopolymer and its biocompatibility [10,11]. The material was lyophilized to constant weight and crushed until flakes were obtained, which were later solubilized in acetic acid pH 3.5 to obtain a 1.5% collagen gel (w/w).

2.2. Nanohydroxyapatite preparation

Solution of 100 mL of 0.01 mol L^{-1} cetrimonium bromide (CTAB) was slowly added to 0.6 mol L^{-1} K_2HPO_4. After addition, pH was adjusted to 12 with NaOH and the mixture was stirred for 2 h. Solution of 1.0 mol L^{-1} $CaCl_2$ was added to the previous solution, under constant stirring. The suspension was refluxed at 100 °C for 6 h, and then sonicated for 1 h. The suspension was centrifuged and washed twice with deionized water and once with ethanol, being then centrifuged. The precipitate was left at 40 °C for 12 h for solvent evaporation, to finally be calcined at 550 °C for 5 h [12].

2.3. Extracts preparation

Grape seed extract (*Vitis* sp.) (P) was obtained from local drugstore.

Pomegranate peel extract (*Punica granatum*) (R) was extracted in 60% hydroethanolic (v/v), with agitation for 1 h, at 50 °C [13]. The suspension was filtered, the filtrate dried under air flow and lyophilized.

Jabuticaba peel extract (*Myrciaria* sp.) (J) was obtained in a similar way, with extraction in 95% hydroethanolic solution (v/v) acidified with 1.5 mol L^{-1} HCl, under agitation for 12 h [14].

The dry powders were solubilized in a 75 mg mL^{-1} solution of ethanol and acetic acid pH 3.5 (1:1).

2.4. Scaffolds preparation

Different gels were prepared under mechanical stirring of 900 rpm, according to the proportions shown in Table 1. The gels were placed in Teflon® molds and neutralized in ammonia vapor for 2 h to obtain eight different scaffolds as shown in Table 1.

Table 1
Scaffolds names and their respective compositions.

Scaffolds	Composition	Proportion (g)				
		C	nHA	P	R	J
C	Collagen	30	–	–	–	–
CP	Collagen + grape seed extract	30	–	5	–	–
CR	Collagen + pomegranate peel extract	30	–	–	5	–
CJ	Collagen + jabuticaba peel extract	30	–	–	–	5
CnHA	Collagen + nHA	30	6	–	–	–
CnHAP	Collagen + nHA + grape seed extract	30	6	5	–	–
CnHAR	Collagen + nHA + pomegranate peel extract	30	6	–	5	–
CnHAJ	Collagen + nHA + jabuticaba peel extract	30	6	–	–	5

2.5. Characterization

2.5.1. Fourier-transform infrared spectroscopy (FTIR)

The chemical structure of fruit extracts was examined by FTIR. Fruit extracts analysis were performed using KBr. All samples were stored in a desiccator with $NaOH_{(s)}$. FTIR spectra were acquired in a Shimadzu IR Affinity-1 infrared spectrophotometer at 4000–400 cm^{-1} interval with 4 cm^{-1} resolution and 32 scans.

2.5.2. Total phenolics content (TPC)

Total phenolic contents (TPC) in grape seed, pomegranate and jabuticaba peel extracts were determined by Folin-Ciocalteu colorimetric method as described by Singleton et al. [15] with minor modifications. The procedure consists in the reduction of a mixture of molybdates and tungstates (Folin's reagent) due to the presence of phenolic species in alkaline medium using gallic acid as standard. The reduction reaction leads to the formation of phenolate anions, blue chromogens with maximum absorbance at 725 nm.

To assess TPC of fruit extracts, 50 μL of the extracts at an initial concentration of 0.05 mg mL^{-1} were mixed with 50 μL of Folin's reagent (Sigma-Aldrich®) in a 96-well plate for 5 min. Then, the medium was alkalized with the addition of 200 μL of a sodium carbonate solution (20%, v/v), and the reaction took place for 15 min in the dark. The plates were quantified by absorbance measurement at 725 nm in an UV–Vis Thermo Scientific™ VL0L00D0 spectrophotometer (Finland). The blank used was an ethanolic solution (50%, v/v) without extracts. The results were expressed in mg gallic acid equivalent (mg GAE) per mg extract based on the calibration curve. All the experiments were carried out in triplicates.

2.5.3. Energy-dispersive X-ray spectroscopy (EDX)

Ca/P ratio was obtained in triplicate by EDX LINK ANALYTICAL equipment (Isis System Series 200), with detector SiLi Pentafet, ultra-thin window ATW II, coupled an Electron Microscope LEO 440, with detector Oxford (Oxford Instruments Inc.). Calcium phosphate was adhered to the stub with conductive tape and coated with carbon. The semi-quantitative analysis was obtained with the ISIS 3.1 software.

2.5.4. X-ray diffraction (XRD)

HA diffractograms were obtained using a Rigaku Rotaflex diffractometer, model: RU200B, with CuKα monochromatic radiation (l = 1.5418 Å) with a power of 40 kV, 60 mA, operated in scanning mode. The sample was scanning speed of 1° min^{-1} and 2θ between 5 and 70° using a step of 0.02°. The diffractogram was compared with standards found in the JCPDS (Joint Committee for Powder Diffraction Studies - HA, JCPDS 9-0432) and the size of the crystals calculated by the Scherrer equation (Eq. (1)), with K equal to 0.94, the length X-ray wave

(λ) equal to 0.154056 nm (CuKα) and β is the width at half the height of the diffraction peak 002.

$$L_{002} = \frac{K \times \lambda}{\beta \cos \theta} \quad (1)$$

The percentage of crystallinity was calculated by Eq. (2), where X_C is the percentage of crystallinity in the sample, $V_{112/300}$ is valley intensity between the diffraction peaks for the planes (112) and (300) and I_{300} is the intensity of the diffraction peak for the plane (300) [16].

$$Xc = \left(1 - \left(\frac{V_{\frac{112}{300}}}{I_{300}}\right)\right) \times 100 \quad (2)$$

2.5.5. Differential scanning calorimetry (DSC)

Thermal stability of scaffolds was determined by differential scanning calorimetry (DSC-2010, TA Instruments) from 5 to 120 °C. Heating was performed in hermetic aluminum pans in nitrogen atmosphere (80 mL min^{-1}) at a rate of 10 °C min^{-1} using 20 mg of sample. Temperature of denaturation was given from the inflection point.

2.5.6. Scanning electronic microscopy (SEM)

Scaffolds and nHA samples were coated with a thin layer of gold of 6 nm. The samples were examined with a Leo 440, LEO Electron Microscope Ltd. with an accelerating voltage of 20 keV. To determine the size of the nHA, Feret's diameter was used in the horizontal (d_H) and vertical (d_V) positions of 50 particles (Fig. S1a and b). The scaffolds pore size was determined using Martin's diameter (Fig. S1c) and measuring at least 40 pores. For the cross-section analysis, the scaffolds were frozen in liquid nitrogen, fractured and lyophilized.

2.5.7. Porosity assays

First, the dimensions of the scaffolds were measured using a caliper and the total volume (V_{total}) was calculated. Then, they were placed in a drying chamber in the presence of $NaOH_{(s)}$ for 24 h, weighed ($W_{inicial}$) and swelled in 10 mL of pure ethanol for 24 h. After this, scaffolds were weighed again (W_{final}) and percentage of porosity was calculated from Eq. (3), with (ρ_{EtOH}) being the density of ethanol (0.790 mg mL^{-1}). The procedure was made in quintuplicate.

$$\%\text{porosity} = \frac{\left(W_{final} - W_{initial}\right)/\rho_{EtOH}}{V_{total}} \times 100 \quad (3)$$

2.5.8. Saline phosphate buffer (PBS) absorption

Scaffolds were placed in phosphate buffered saline (PBS). At specific time intervals, they were removed and the excess of solution was removed using a 2 cm × 2 cm filter paper. The scaffolds were weighed and returned to PBS for further time taken. The percentage of PBS absorbed was calculated by averaging the results found using Eq. (4), where w_{humid} is the mass of the swollen scaffold and w_{dry} is the mass of the scaffold before swelling. The process was made in quintuplicate.

$$\%\text{absorption} = \frac{w_{humid} - w_{dry}}{w_{dry}} \times 100 \quad (4)$$

2.5.9. Collagenase degradation assays

Collagenase solution (10 U mg^{-1} of collagen) in 10 mmol L^{-1} tris-HCl buffer at pH 7.4 containing 25 mmol L^{-1} $CaCl_2$ was prepared. This solution was added in scaffolds known weights which were incubated at 37 °C for 2 h and 6 h. The samples were washed in deionized water, frozen and lyophilized to constant weight. The percentage of degraded collagen was determined by the difference in collagen mass before ($w_{initial}$) and after enzymatic degradation (w_{final}) by Eq. (5). The process was made in quintuplicate for both times.

$$\%\text{degradation} = \frac{m_{initial} - m_{final}}{m_{initial}} \times 100 \quad (5)$$

2.5.10. Scaffolds sterilization

Scaffolds were individually packaged into double plastic envelopes and sent to Nuclear and Energy Research Institute (IPEN/CNEN). The samples were irradiated in a Cobalt-60 Multipurpose Gamma Irradiator, at 15 kGy (5 kGy h^{-1}) for sterilization and the irradiation protocol was based on the International Organization for Standardization 11.137 [17]. Thermal stability of collagen scaffolds was determined by DSC before and after irradiation with Cobalt-60 and no changes in collagen structure was observed at 15 kGy (data not shown).

2.6. Antimicrobial activity assay

2.6.1. Culture preparation

Staphylococcus aureus ATCC 25923, *Pseudomonas aeruginosa* ATCC 27853 and *Salmonella enterica* Enteriditis ATCC 13076 were maintained on frozen glycerol stocks. *S. aureus* was grown on tryptic soy agar (TSA, Acumedia) containing 6 g L^{-1} of yeast extract. *P. aeruginosa* and *S.* Enteritidis were streak on nutrient agar (NA, Himedia). Cultures were grown overnight at 37 °C. After incubation, some colonies were suspended in saline solution (NaCl 0.86%) and adjusted to approximately 10^8 CFU mL^{-1} at the onset of subsequent experiments to ensure that cultures were in the exponential growth phase.

2.6.2. Determination of minimum inhibitory concentration (MIC) and minimum bactericidal concentration (MBC) of the crude extracts

MIC and MBC of grape, pomegranate and jabuticaba extracts against bacterial strains were performed using the broth microdilution assay according to CLSI guidelines [18]. The extracts (dissolved in 1% dimethyl sulfoxide - DMSO) were prepared in Müeller Hinton broth (MHB, Himedia) at an initial concentration of 2000 μg mL^{-1} and then serially diluted (twofold) in a 96-well plate. A 20 μL aliquot of standardized inoculum at a final concentration of 10^7 CFU mL^{-1} was added to all the wells except for the negative control. Inoculated MHB culture medium with and without 1% DMSO were also included as controls. The microplates were then incubated at 37 °C for 24 h, and a comparison with the positive control was performed by visual inspection to assess growth. To confirm the presence or absence of growth, 20 μL of 0.1% 3-[4,5-dimethylthiazol-2-yl]-2,5-diphenyl tetrazolium bromide (MTT) solution was added to the wells.

Before adding MTT, 10 μL of wells with no apparent growth were spotted onto TSA (or NA) plates and incubated again for 24 h. The lowest sample concentration with no apparent growth was identified as the MIC and the lowest concentration with no detectable viable cells was identified as the MBC. All assays were performed in at least three independent replicates.

2.6.3. Antimicrobial activity of scaffolds

The determination of the inhibition effect of the scaffolds against *S. aureus* ATCC 25923 was carried out using disk diffusion method [19]. Scaffolds (15 mm) were applied on the surface of plates, containing Müeller Hinton agar (MHA, Himedia) previously streaked with the bacterial suspension adjusted to 0.5 McFarland (10^8 CFU mL^{-1}) standard. Filter paper disks (5 mm) impregnated with 20 μL of ampicillin (50 μg mL^{-1}) were used as control. Plate readings were taken after 24 h of incubation at 37 °C.

2.7. Cytotoxicity assay

The cell line NIH/3T3 (ATCC CRL 1658) was used in the MTS assay. Solutions of vegetal extracts and nanohydroxyapatite were prepared at 1.250, 0.625, 0.312 and 0.156 mg mL^{-1} concentrations with Dulbecco's Modified Eagle Medium (DMEM) (Gibco, Invitrogen). The cytotoxicity of the scaffolds was evaluated by the indirect contact assay [20] where the cells were cultured with extracts from the materials that make up the scaffolds, i.e., cell medium that had been in contact with each material individually. The scaffolds were placed in a test tube, culture medium

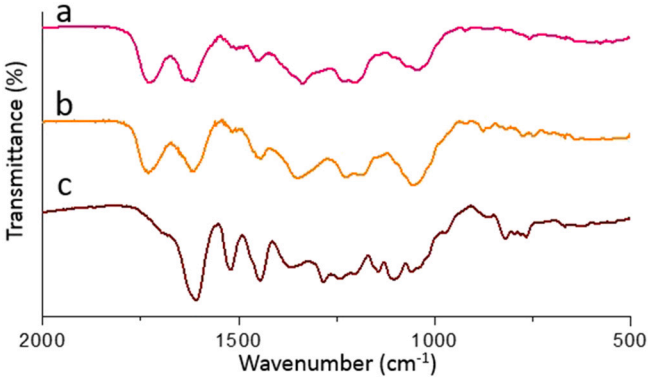

Fig. 1. FTIR spectra (a) jabuticaba peel, (b) pomegranate peel and (c) grape seed extracts.

was added at a ratio of 0.1 g/mL (mass of scaffold per volume of culture medium) and incubated in 5% CO_2, at 37 °C for 24 h, after which, the scaffolds were removed from the media and 100% extract were obtained.

Cells were seeded on 96-well plates (5×10^5 cells mL^{-1}) in DMEM, supplemented with 10% fetal bovine serum and incubated for 24 h at 37 °C in 5% of CO_2. Subsequently, culture medium was removed and 100 μL of vegetal extracts solutions, nanohydroxyapatite solutions and the scaffolds extracts were added to each well. The plates were incubated for 24 h and 48 h, at 37 °C and 5% CO_2. After 24 h and 48 h, the broth (supernatant) was removed, the cells were washed with PBS, and each well was filled with fresh medium containing 50 μL of MTS (3-(4,5-dimethylthiazol-2-yl)-5-(3-carboxymethoxyphenyl)-2-(4-sulfophenyl)-2H-tetrazolium) (1 mg mL^{-1}). The plate was incubated for 4 h under the conditions described above. Then, the medium was replaced with 100 μL of 2-propanol, and the optical density (OD) was measured at 490 nm using a spectrophotometer Biotek Synergy HT microplate reader. The cytotoxicity was expressed as the percent reduction in absorbance of treated cells relative to untreated control. All assays were performed in quintuplicate for both times.

2.8. Statistical analysis

Quantitative data are presented as the mean ± standard deviation (SD). Statistical analyses were performed by one-way ANOVA or Student's *t*-test. $p < 0.05$ was considered significant between two groups of data.

3. Results and discussion

3.1. Fourier transform infrared spectroscopy (FTIR)

Fourier transform infrared spectroscopy was used to identify the functional groups present in the different fruit extracts. The FTIR spectra of the extracts are shown in Fig. 1. The broad bands observed at 3400 cm^{-1} correspond to stretching vibrations of flavonoids hydroxyls (O—H) groups. The characteristics bands at 1728 cm^{-1} (R) and 1737 cm^{-1} (J) can be attributed to the C═O stretching of ketones, which can be assigned to the presence of some flavonoids in the pomegranate and jabuticaba extracts, except for proanthocyanidin, abundant in grape seed extract [21]. The bands near to 1615 cm^{-1} and those of less intensity close to 1514 cm^{-1}, correspond to the stretching of the aromatic ring C=C–C. The C═C stretching of the aromatic ring is also observed close to 1449 cm^{-1}. In the region from 1244 to 1230 cm^{-1}, the characteristics bands correspond to the C—O stretching of the pyran ring present in the flavonoids, while the observed band close to 1050 cm^{-1} is due to the C—O stretching of alcohols [22].

3.2. Total phenolics content (TPC)

The Folin Ciocalteu method is a way to evaluate the total phenolic content of different fruit extracts and assess their antioxidant power by directly comparing of phenolic hydroxyls available.

According to the results obtained, grape seed extract (TPC of 597 ± 53 mg GAE g $extract^{-1}$) presented almost twice the total phenolic content compared to jabuticaba peel (TPC of 315 ± 20 mg GAE g $extract^{-1}$) and pomegranate peel (TPC of 332 ± 8 mg GAE g $extract^{-1}$) extracts. Rodrigues et al. [8] reported similar values for grape seed and jabuticaba peel extracts. In addition, the values found for the extracts in our study were higher than most authors report [23,24], which is a good result for future applications in the development of materials.

The differences in the TPC of different extracts could be due to several factors, such as the type of fruit, its variety and stage of maturation, species and seasonality, as well as the different kind of extraction method and solvents used [8]. Moreover, the highest phenolic content observed for the grape seed extract can explain its greater interaction with collagen/nAH scaffold. The greater the hydroxyls availability of the extract, the greater the interaction. It is believed that the extracts addition to the polymer matrix established bonds between the phenolic hydroxyls and the polymer groups, including hydrogen, hydrophobic and covalent bonds.

Overall, these results showed the potential use of different extracts for the development scaffolds with improved features based on the type

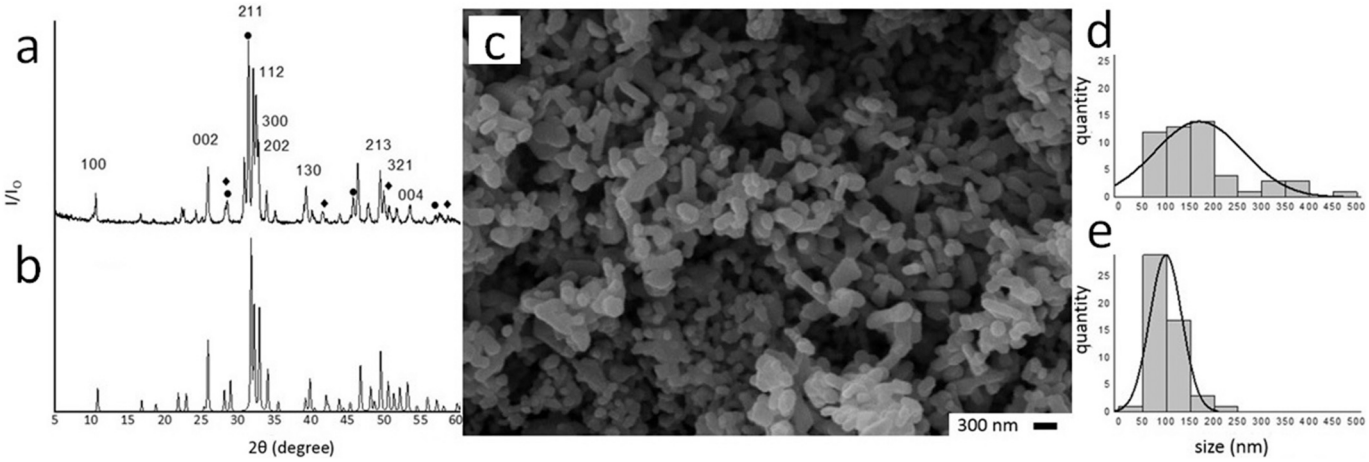

Fig. 2. Diffractograms of a) synthesized hydroxyapatite, with (•) NaCl and (◆) KCl peaks; b) JCPDS 9-0432 hydroxyapatite; c) nanohydroxyapatite photomicrograph; d) horizontal diameter histogram; e) vertical diameter histogram.

Table 2
Collagen denaturation temperature values (Td °C) for the scaffolds.

Scaffolds	Td (°C)
C	47.6
CP	59.2
CR	52.8
CJ	53.2
CnHA	47.9
CnHAP	56.6
CnHAR	52.8
CnHAJ	52.2

of application to be given to the material. In the case of bone regeneration, it is interesting that the extracts incorporation increases the resistance of scaffolds to enzymatic degradation, prolong their release with cytotoxic effect reduced and antibacterial action over time, and that the extracts phenolic compounds are available to overcome the polymeric matrix oxidation.

3.3. Energy-dispersive X-ray spectroscopy (EDX)

The Ca/P ratio of calcium phosphate was obtained by EDX, being 1.60 ± 0.03. This value is closer to hydroxyapatite (Ca/P = 1.67) than to amorphous apatites (Ca/P = 1.50) and tetracalcium phosphate (Ca/P = 2.0) [25]. It was also observed the presence of small peaks referring to sodium in 1.02 keV, chlorine in 2.62 keV and potassium in 3.30 keV, present in the precursors of the synthesis.

3.4. X-ray diffraction (XRD)

Diffractograms (Fig. 2a and b) showed characteristic diffraction peaks when compared with the JCPDS 9-0432 standard, confirming that the synthesized calcium phosphate was hydroxyapatite. Diffraction

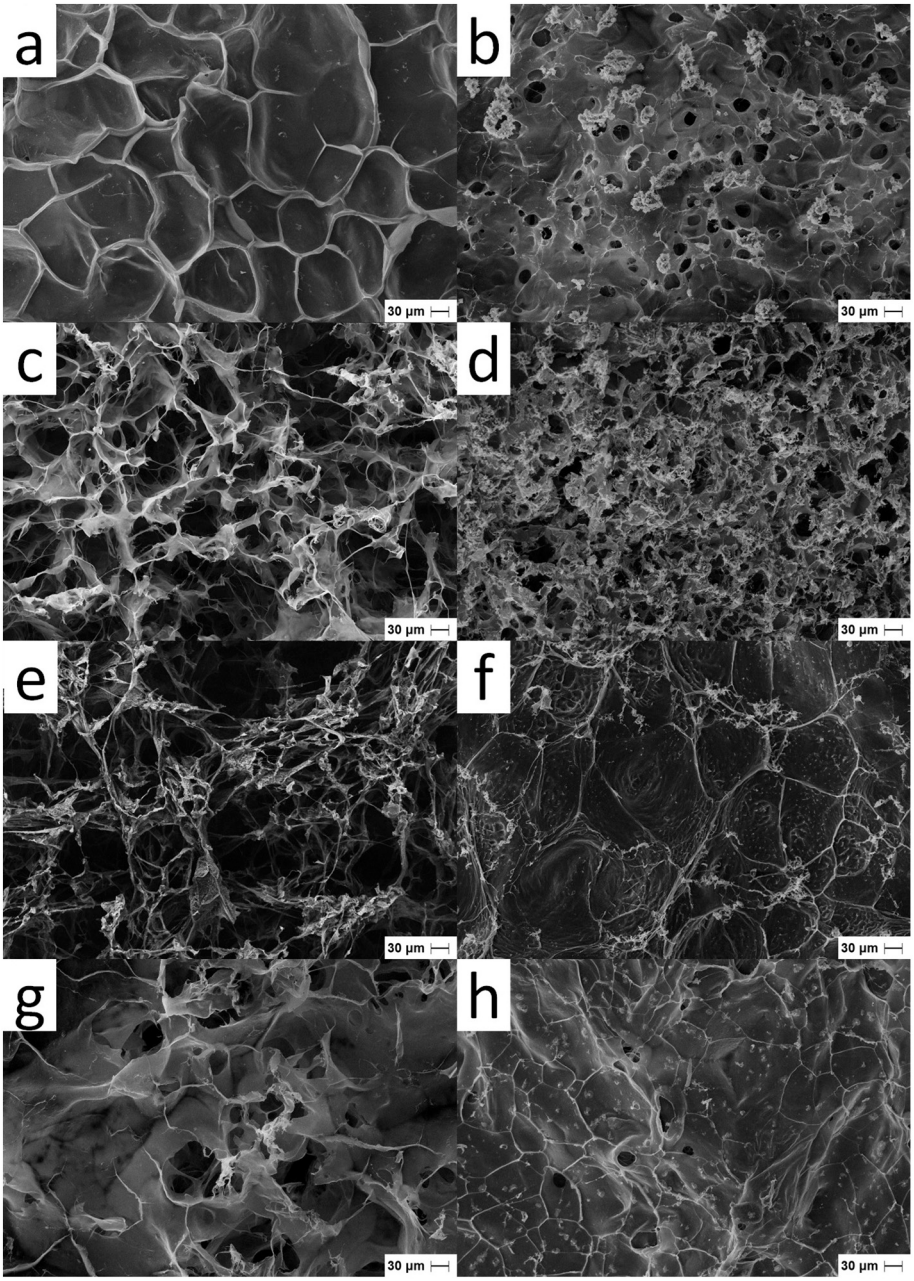

Fig. 3. Surface photomicrographs of: a) C; b) CnHA; c) CP; d) CnHAP; e) CR; f) CnHAR; g) CJ; h) CnHAJ at 500× magnification.

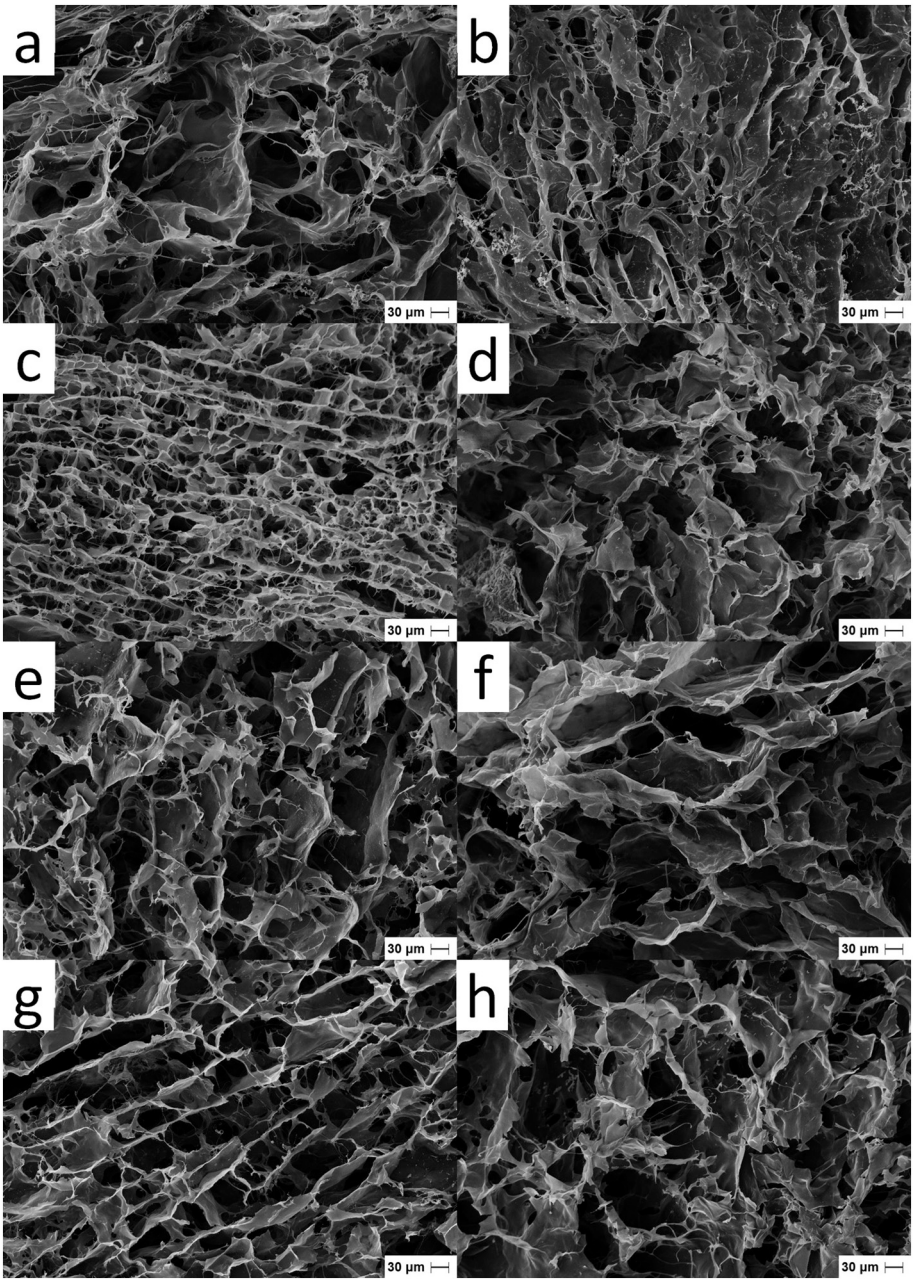

Fig. 4. Cross-sectional photomicrographs of: a) C; b) CnHA; c) CP; d) CnHAP; e) CR; f) CnHAR; g) CJ; h) CnHAJ at 500× magnification.

peaks of NaCl and KCl were also observed in the hydroxyapatite diffractogram, showing the presence of these salts.

According to the Scherrer equation, the size of the crystalline grain was 38.9 nm, and the percentage of crystallinity calculated by Eq. (2) was 80.4%. Although several studies reported that amorphous calcium phosphates have improved bioactivity compared to crystallized calcium phosphates such as hydroxyapatite, they have not considered the different size -effects of calcium phosphates. Hu et al. [26] observed that the smaller nanocrystallites the greater the effect on bone marrow mesenchymal stem cells proliferation. This report led to believe that the high crystallinity found in our study can help in cell growth and differentiation once the hydroxyapatite dimensions are directly related to its bioactivity.

3.5. Scaffold obtaining

The scaffolds presented touch-resistance appearance and they could undergo reversible shape when exposed to small deformations. The extracts presence was visually noted in scaffolds by color: CP and CnHAP are brown, CR and CnHAR are yellow and CJ and CnHAJ are purple. C and CnHA scaffolds are white.

3.6. Differential scanning calorimetry (DSC)

The anionic collagen was prepared by alkaline hydrolysis, which produces a negatively charged anionic collagen matrix at pH 7.4. This can be done by the hydrolysis of carboxyamide groups of asparagine (Asn) and glutamine (Gln) increasing the number of negative charge present in the α chains of type I collagen, without affect the integrity of the collagen triple helix structure [10,11]. The increase in the number of negative charges could lead to an interaction of collagen with nano-HA, however, this was not observed by DSC as shown in Table 2.

An increase in the denaturation temperature of the scaffolds containing extract (CP, CR and CJ) was observed compared to scaffold C,

Table 3
Pore size values obtained by SEM photomicrographies.

Scaffolds	Smallest (μm)		Largest (μm)		Mean ± sd (μm)		Cv (%)	
	Surface	Internal	Surface	Internal	Surface	Internal	Surface	Internal
C	–	17.0	–	213.2	–	$58.3 \pm 28.7^{d,e}$	–	49.3
CP	23.0	23.0	112.9	220.2	$56.3 \pm 23.9^{b,c}$	$60.9 \pm 33.8^{c,d,e}$	42.4	55.4
CR	32.1	31.0	449.9	169.9	126.1 ± 118.6^{a}	$69.9 \pm 26.7^{b,c,d}$	94.0	38.2
CJ	20.3	26.9	223.7	202.8	72.8 ± 47.1^{b}	$80.9 \pm 45.1^{a,d}$	64.7	55.8
CnHA	15.3	20.2	47.9	67.8	28.1 ± 7.5^{c}	34.7 ± 12.5^{e}	26.6	36.1
CnHAP	16.0	34.9	128.0	226.8	$47.1 \pm 24.2^{b,c}$	97.6 ± 55.6^{a}	51.4	56.9
CnHAR	–	24.0	–	182.7	–	$87.0 \pm 38.0^{a,c}$	–	43.7
CnHAJ	–	34.9	–	229.5	–	$89.4 \pm 43.2^{a,b}$	–	48.4

In the table, equal letters mean statistically equal values ($p < 0.05$).

indicating that the extracts, abundant in flavonoids, act as biopolymer crosslinking agents.

The scaffold with grape seed extract showed a higher denaturation temperature, varying 11.6 °C in relation to C and indicating that the crosslinking with grape seed extract was more effective. CR and CJ have a similar Td, with an increase of about 5 °C.

Flavonoids are molecules that can present several hydroxyl groups which are able to form hydrogen bonds between the amide clusters of the proline residues present in the collagen triple helix, promoting the crosslinking, as observed in all cases [27]. For the hydroxyapatite scaffolds, no difference was observed in Td when compared to the respective scaffolds without hydroxyapatite, except for the CP and CnHAP set which showed a slight decrease of 2.6 °C.

3.7. Scanning electron microscopy (SEM)

The photomicrograph shown in Fig. 2c reveals typical morphology of hydroxyapatite clusters [12]. The mean of 50 determinations, considering the horizontal diameter of the particles was 168.6 ± 92.8 nm and for the vertical diameter was 98.4 ± 33.6 nm. Fig. 2d and e shows horizontal diameter histogram and vertical diameter histogram, respectively.

As size decreases, the surface/volume ratio of the particle increases, which is particularly important as it improves protein sorption and cell adhesion by scaffolds composed of collagen and nanohydroxyapatite [28].

Figs. 3 and 4 show the surface and cross-sectional photomicrographs of the scaffolds, respectively. They have pores on the surface (apart from C, CnHAR and CnHAJ) and internal pores. The size of the largest and smallest pore, together with the mean value and the Cv (coefficient of variation) are shown in Table 3.

CR scaffold showed the greatest variation in the pore size of the surface (Cv = 94%), while the CnHA scaffold showed the smallest variation (Cv = 26.6%). For cross-section, CnHAP scaffold has the biggest pores size variation, presenting Cv = 56.9%.

SEM images of the cross-section scaffolds show a variation from 17 to 229.5 nm in the internal pores size, but it was observed that the average values are closer than those obtained for the surfaces (Table 3).

The cross-sectional photomicrographs of scaffolds without and with nHA revealed that internally the pores are statistically equal, except for CnHA. For the latter, the variation in the pore size of both the surface and internally are less pronounced.

The ideal pore size for bone growth is not a consensus in the literature, as different pore sizes can act in different ways in ossification. Azami et al. [29] reported that the desirable pore size for bone cell growth is between 150 and 350 μm, while Oryan et al. [30] observed scaffolds with pores between 200 and 350 μm as ideal for bone growth and osteoconduction. These authors also concluded that the distribution, pore volume and interconnectivity are equally important factors. Zhao et al. [31] highlighted that the ideal size for a bone reconstruction scaffold is between 300 and 900 μm.

On the other hand, it has been reported that pores smaller than 100 μm may have advantages in bone growth. A pore diameter of 5 μm can provide benefits for cell adhesion and protein adsorption of the material [32]. To address this, Billström et al. [33] have proposed that biomaterials with pores between 0.5 and 10 μm induced the growth of osteogenic cells, leading to the bone formation. Zhang et al. [34] concluded that scaffolds with small diameter pores help in cell attachment and can provide a capillary force that helps in the retention of physiological fluids and guide the cells along the scaffold interior, resulting in bone formation closely integrated with the bone biomaterial.

Table 4
Physical-chemical parameters of scaffolds.

Scaffolds	Porosity (%)	% absorption of PBS		% degradation	
		120 min	1440 min	2 h	6 h
C	92.01 ± 3.87^{a}	$977.4 \pm 109.3^{d,e,f}$	$1337.2 \pm 83.5^{c,d}$	7.53 ± 1.49^{c}	27.63 ± 4.11^{a}
CP	89.03 ± 1.78^{a}	1365.7 ± 108.2^{b}	$1720.2 \pm 105.6^{b,c}$	–*	–*
CR	92.98 ± 2.55^{a}	$1173.9 \pm 187.2^{b,d,e}$	$1621.0 \pm 131.3^{b,c}$	5.37 ± 2.10^{c}	$7.66 \pm 1.26^{c,d}$
CJ	96.23 ± 1.95^{a}	2349.7 ± 283.6^{a}	3057.1 ± 267.6^{a}	4.01 ± 2.28^{c}	3.98 ± 0.62^{d}
CnHA	90.77 ± 3.39^{a}	652.1 ± 146.7^{f}	990.8 ± 210.6^{d}	22.70 ± 3.00^{a}	29.68 ± 2.65^{a}
CnHAP	90.55 ± 1.67^{a}	2554.6 ± 220.0^{a}	2769.7 ± 214.3^{a}	4.33 ± 1.37^{c}	16.31 ± 4.22^{b}
CnHAR	64.71 ± 7.11^{b}	$883.2 \pm 138.2^{c,e,f}$	1103.9 ± 158.5^{d}	16.45 ± 0.15^{b}	$14.33 \pm 2.06^{b,}$
CnHAJ	73.86 ± 4.10^{b}	$1278.9 \pm 129.9^{b,c,d}$	2033.5 ± 342.2^{b}	13.79 ± 0.05^{b}	$12.18 \pm 2.4^{b,c}$

In the same column, equal letters mean statistically equal values ($p < 0.05$).
* Degradation was not observed.

Karageorgiou et al. [35] found a pore diameter of 100 μm as ideal for cell migration and larger than 300 μm as more suitable for the bone formation. These data are in agreement with Murphy et al. [36] who demonstrated that pores larger than 300 μm accelerate the osteogenesis, and smaller than 300 μm, induce endochondral ossification. However, endochondral ossification also requires small pieces of cartilage are needed to serve as a "mold" to be completely replaced by new bone. Similar findings were reported by Velasco et al. [37] who demonstrated that pores of approximately 100 μm allow chondrogenesis, while pores of approximately 350 μm promote osteogenesis.

Considering all these authors, it is possible to conclude that the CP, CR, CJ and CnHAP scaffolds can be promising for osteogenesis due to their smaller pores (100 μm), which help in cell adhesion and the swelling of the scaffold. The scaffolds also had pores larger than 100 μm that can be beneficial for osteogenesis and appropriate internal structures, except for CnHA. In addition, collagen and nanohydroxyapatite are bioabsorbable and biodegradable, which when post-implantation, should be degraded continuously in vivo and modify the pore size [38].

3.8. Porosity assay

Porosity, as well the pore diameter, shape, and interconnectivity, has important effects on biomaterial preparation for bone tissue reconstruction.

Scaffolds porosity is shown in Table 4 and it is possible to notice values around 90%, except for CnHAR and CnHAJ, which porosity values significantly decreased.

Fook et al. [39] reveled that porosity values above 70% are an essential characteristic for bone implants based on biomaterials. On the other hand, Zhao et al. [31] reported a wider range of porosity between 60 and 95% for a bone growth scaffold.

It was observed for the scaffolds without nHA that the addition of extract had no influence in the porosity, as well as CP, CR and CJ did not show significant difference between their porosities.

As the collagen concentration was reduced in the scaffolds, the porosity decreased, as observed in the CnHAR and CnHAJ, which presented 64.71 ± 7.11 and 73.86 ± 4.10%, respectively. However, this difference was not observed for CnHAP. These results can be explained based on the predominance of proanthocyanins in the grape seed extract [21], which can be present in the form of dimers or trimers and, therefore, can cross-link collagen without getting too close the biopolymer chain. For pomegranate and jabuticaba peel extract, the most abundant flavonoids are catechins (flavanols) and anthocyanins [40,41] that come in the form of monomers. Collagen is also crosslinked by these monomers; nevertheless, they can cause a greater effect in the collagen chain approximation, reducing scaffold porosity [42,43].

3.9. Saline phosphate buffer (PBS) absorption

Table 4 shows the absorption values of scaffolds after 120 min and 1440 min, while Fig. S2 shows their absorption (a) without nHA and (b) with nHA.

It was observed that in 1440 min, CnHA scaffold showed the lowest absorption of PBS, with no statistical difference compared to C scaffold, indicating that only the addition of nanohydroxyapatite at the concentration tested did not induce an increase in absorption.

Kozlowska et al. [44] tested the absorption of PBS by collagen scaffolds with hydroxyapatite in different proportions. They found that with the increase in the amount of hydroxyapatite in the scaffold, the absorption of PBS was lower. However, in our study, the amount of hydroxyapatite in the CnHA scaffold was lower than evaluated by Kozlowska et al. [44], indicating that the increase in nHA concentration may result in a statistical difference in the absorption of C and CnHA scaffolds.

In comparison, the absorption of PBS by C, CP and CR scaffolds was not influenced by the addition of grape seed or pomegranate peel extracts, since all the values are statistically equal in the period of 24 h. However, the addition of jabuticaba extract significantly increased the absorption.

The crosslinking of collagen scaffolds does not always change the percentage of PBS absorption, as shown by Sionkowska and Grabska [45]. The authors tested the absorption of collagen and crosslinked collagen scaffolds with dialdehyde starch and obtained values of 1055% and 1084%, respectively.

When nanohydroxyapatite was added to the grape seed extract scaffold, there was a significant increase in PBS absorption, however for pomegranate and jabuticaba extract scaffolds, the nHA addition resulted in the opposite effect, reducing the percentage of scaffold absorption. Like to C and CR scaffolds, the percentage of absorption for CnHA and CnHAR was the same.

3.10. Collagenase degradation assays

The selection of bone reconstruction biomaterials is also based on their biodegradability. Ideally, the degradation rate of bone biomaterials should match the growth rate of new bone, without generating harmful degradation products to osteogenesis [46]. The collagenase assay may be indicative of the biodegradability of post-implant biomaterial. Table 4 presents the percentage of scaffolds degradation after 2 and 6 h.

There was a difference in the rate of degradation, depending upon the stability of the individual scaffolds. The rate of degradation of C, CnHA and CnHAP scaffolds increased as a function of time with greater degradation after 6 h. For the other samples it was observed that the extracts addition reduced the collagen percentage of degradation, except for the CP scaffold, which did not degrade. These data offer some indications that the extracts act as collagen crosslinking agents, being the grape seed extract that one with the highest crosslinking capacity, which is consistent with the fact that the CP scaffold has a higher denaturation temperature. These results indicate that the extracts stabilized the crosslinked collagen against collagenase activity.

Similar findings were also presented by Green et al. [47] who used the proanthocyanins from grape seed extract in collagen adhesives in periodontal regeneration. They concluded that the biopolymer was crosslinked by the extract, which reduced its biodegradation.

For C and CnHA, it was observed that the nanohydroxyapatite addition increased the degradation percentage of collagen, indicating that bioceramics may destabilize the scaffold. However, the values obtained after 6 h were not statistically higher than those observed after 2 h. When comparing CP with CnHAP, CR with CnHAR and CJ with CnHAJ, at both times, scaffolds with hydroxyapatite showed greater degradation, indicating the destabilization caused by bioceramics, mainly for CnHAP. The increased degree of degradation can be attributed to the presence of positive charged ions such as Ca^{2+} in hydroxyapatite that have an affinity for the collagen anionic fibers and can cause a destabilization via physical interactions among the collagen fibers [48].

Therefore, the increased stability of collagen scaffolds against collagenase following the extracts addition highlights its importance in the collagen-based biomaterials development for tissue engineering applications.

Table 5
MIC and MBC values of grape seed, pomegranate peel and jabuticaba peel extracts.

Strains	Grape seed extract		Pomegranate peel extract		Jabuticaba peel extract	
	MIC	MBC	MIC	MBC	MIC	MBC
	μg mL^{-1}					
S. aureus	250	250	500	500	1000	2000
P. aeruginosa	>2000	>2000	>2000	>2000	>2000	>2000
S. Enteritidis	>2000	>2000	>2000	>2000	>2000	>2000

3.11. Antimicrobial activity assay

3.11.1. Antimicrobial activity of the extracts

The MIC and MBC of grape, pomegranate and jabuticaba extracts were evaluated against planktonic cultures of *S. aureus*, *P. aeruginosa* and *S.* Enteritidis. As shown in Table 5, all the extracts affected *S. aureus* growth, but the grape seed extract was the most effective comparatively to the others. However, none of them were able to inhibit the growth of Gram-negative strains at the concentrations tested. The difference in efficacy against Gram-positive and -negative species is probably due to the presence of outer membrane in Gram-negative bacteria, which confers low permeability to hydrophobic molecules like the extracts.

Antimicrobial activity of plant extracts has been attributed to flavonoid contents [49] but natural variations in their chemical profiles like the amount of phenolic compounds may be responsible for the observed differences in antimicrobial effectiveness. Our results are in agreement with previous reports regarding better antimicrobial efficacy

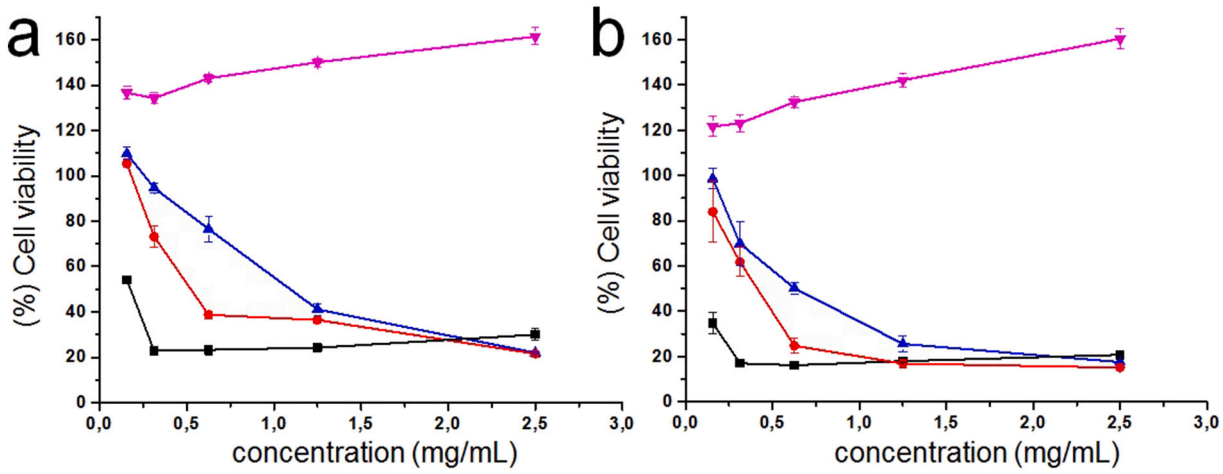

Fig. 5. Percentage of cell viability in: a) 24 h and b) 48 h, for (▼) nHA; (■) P; (●) R; (▲) J.

of flavonoids against Gram-positive bacteria [50,51]. It should be noted, however, that the MIC and MBC values measured in this study for the extracts against *S. aureus* ATCC 25923 were 2- to 40-fold lower than in other studies [52,53].

Hence, our data demonstrated that flavonoids from grape seed, pomegranate peel and jabuticaba peel extracts displayed a potential antimicrobial action against *S. aureus* possibly by interacting with peptidoglycan in the cell wall [54].

3.11.2. Antimicrobial properties of the scaffolds

For orthopedic implants *Staphylococcus aureus* infections are the most prevalent [55]. The common involvement of *S. aureus* in infections has led to extensive treatment with many different antibiotics, and thus evolvement of multi-resistant strains [56]. Because the scaffolds can be used as possible agents to avoid contaminants during surgeries, we evaluated the antimicrobial activity of collagen and collagen/nano-hydroxyapatite scaffolds with and without extracts addition against *S. aureus* by the disk diffusion method.

Inhibition zone was only observed for collagen/pomegranate peel extract scaffold with 18.6 ± 2.3 mm. However, all the crude extracts resulted in activity against *S. aureus* as noted above using the broth dilution method. This is partly due to due to lack of (or delayed) diffusion of antimicrobial into agar and some limitations of the test to obtain a homogenous set. Moreover, the extracts work as a collagen cross-linking agent and should be physically or chemically linked to the polymeric structure, reducing its diffusion in the medium and thus resulting in the absence of inhibition zone [57]. This is a good result aiming the potential application of these scaffolds in bone tissue engineering, since the scaffolds with extracts have a suitable degradation rate as shown in Table 4, and may release the embedded extracts, which play a key role in the antimicrobial activity of these materials.

There are many reports in the literature showing a dose dependent inhibitory effect on *S. aureus* where increasing the concentration of the extracts in the scaffold increased the zone of inhibition [58,59]. In other studies, the antimicrobial activity was performed using the crude extracts spotted directly on the surface of agar or filter paper disks impregnated with the extracts, enhancing the antibacterial efficacy [59].

These results are very encouraging for the outlook of using antimicrobial scaffolds combined with bioactive molecules that are based on flavonoids together with other approaches in the treatment of bone infections against *S. aureus*.

3.12. Cytotoxicity assay

Selective toxicity is important to the design of bone biomaterials thus, we evaluate the cytotoxicity of crude extracts and nano-hydroxyapatite against mouse fibroblasts (NIH/3T3; ATCC CRL 1658).

3.12.1. Cytotoxicity of plant extracts and nanohydroxyapatite

Fig. 5 shows the cell viability values for plant extracts and nHA.

Hydroxyapatite is widely used as a biomaterial for regeneration of hard tissue due to its biocompatibility, therefore it was expected that it did not present cytotoxicity [4]. It is also observed that with the increase in the nanohydroxyapatite concentration, there was an increase in the cell viability reaching close to 160% for both times, indicating that the synthesized nanohydroxyapatite has proliferative properties and good biocompatibility, and can be a potential biomaterial for tissue reconstruction.

Pomegranate and jabuticaba peel extracts have proliferative properties at concentration of 0.156 mg mL^{-1} (24 h of incubation), differently the grape extract showed cytotoxicity in the same period. After 48 h, only jabuticaba extract showed non-cytotoxic properties at this concentration. Higher concentrations of all compounds, however, resulted in decrease in the cell viability for both periods.

The ability of flavonoids to remove free radicals can be an explanation for the cytotoxic activity observed for the extracts at higher concentrations [60]. In addition, the cytotoxic activity of the extracts as well as the antimicrobial activity can be influenced by the environmental conditions in which the fruits were obtained [49], by the extract extraction process and also by the concentration range tested. Many researchers found different cytotoxicity values for extracts of the same fruit [61,62].

Okonogi et al. [61] evaluated the cytotoxicity of the pomegranate peel extract, extracted in 95% hydroethanolic solution for 3 days. They reported that up to a concentration of 0.1 mg mL^{-1} the extract was able to increase the cell viability of Caco-2 cells (cell line of human colorectal epithelial adenocarcinoma cells).

Pitz [62] evaluated the cytotoxicity of jabuticaba extract and concluded that at concentrations of 100 μg mL^{-1}, the extract showed proliferative properties. On the other hand, at concentrations of 200 μg mL^{-1}, the extract was cytotoxic. In this study, the lowest concentration of extract tested was 0.156 mg mL^{-1}, resulting in cell viability of 105.5 ± 1.8 and 109.8 ± 2.8% after 24 h, for pomegranate and jabuticaba extracts, respectively. Our results are in line with those described by Pitz [62] in the literature about the relationship between the cell viability and the extracts concentrations.

For the grape seed extract the cell viability decreased between the concentrations of 0.156 and 0.312 mg mL^{-1} and increased at 2.5 mg mL^{-1} concentration after 24 h of incubation. After 48 h, the decrease in cell viability occurred until the concentration of 0.625 mg mL^{-1}, and after that concentration there was an increase in viability, indicating

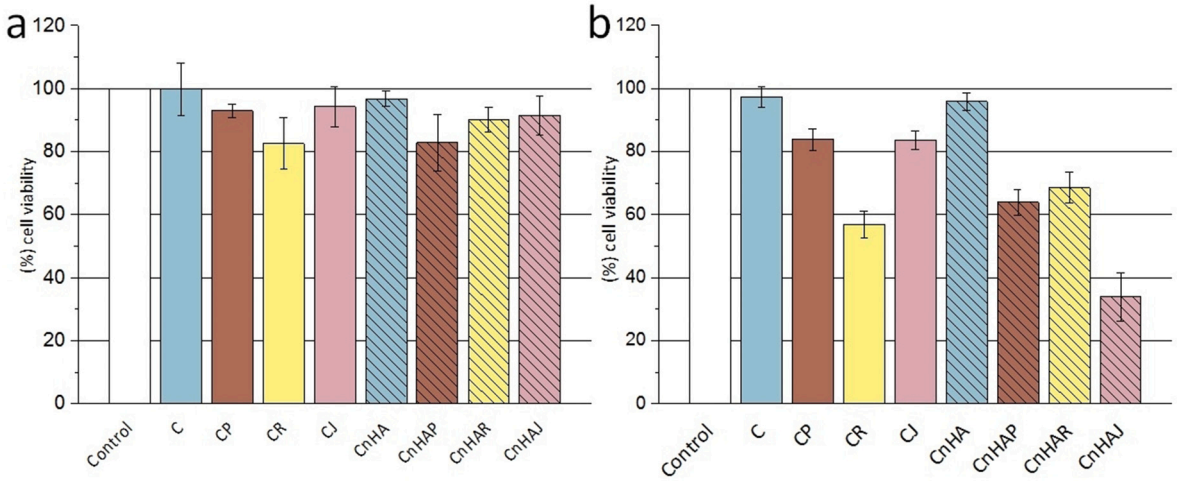

Fig. 6. Percentage of cell viability after a) 24 h and b) 48 h for the scaffolds.

that within the concentration range the compounds had higher cytotoxicity, but when the concentration tested exceed this range none of the compounds were toxic.

3.12.2. Cytotoxicity of scaffolds

Fig. 6 shows the percentage of cell viability for the scaffolds after 24 and 48 h of incubation. It was observed that after 24 h, all the scaffolds did not show cytotoxicity. Padrão et al. [25] reported similar results for heparinized nanohydroxyapatite/collagen combined with antibiotic. However, after 48 h, CR, CnHAP, CnHAR and CnHAJ scaffolds were cytotoxicity.

At both time points, C and CnHA scaffolds had the highest cell viability (higher than 90%). Thus, there is an indication that the addition of plant extracts in the scaffolds can reduce the cell viability.

Huang et al. [63] studied the cytotoxicity of proanthocyanidin incorporated in gelatin nanofibers against mouse fibroblast cells L-929. For this, they cultivated the cells directly on the material and as a result, they found that this incorporation not only accelerated the cell proliferation, but also increased the efficiency of drug loading.

The study of these authors suggests that the use of plant extracts in biomaterials can be promising, and the concentration reduction of these extracts can increase the cell viability. Nevertheless, C, CP, CJ and CnHA scaffolds did not show cytotoxicity in both periods, proving favorable to their use as biomaterials.

4. Conclusion

This study demonstrates that the extracts act as collagen crosslinking agents, increasing its thermal stability and enzymatic resistance; the scaffolds presented pore size and porosity suitable for the growth of bone tissue. All the extracts showed antimicrobial activity and inhibition zone was observed for CR scaffold against *S. aureus*. It was also noticed a high influence of the extract over cytotoxicity of the scaffolds. However, C, CP, CJ and CnHA scaffolds were not cytotoxic after 48 h, representing therefore one more way to control its properties during the preparation of new materials. Moreover, results are promising to development of scaffolds trough the combination of bioactive molecules as biomaterials to provide better outcomes for bone regeneration.

Funding

This study was supported by the National Council for Scientific and Technological Development (CNPq) contract number 130686/2018-2 (Msc grant for CFG), by the Coordenação de Aperfeiçoamento de Pessoal de Nível Superior (CAPES) (PhD grants for CAM and LCM).

Consent for publication

The authors have consented for publication.

Ethics approval and consent to participate

Not applicable.

CRediT authorship contribution statement

Claudio Fernandes Garcia: Conceptualization, Methodology, Data curation, Writing - Original draft preparation
Crisiane Aparecida Marangon: Data curation, Writing - Original draft preparation
Lívia Contini Massimino: Data curation, Writing - Original draft preparation
Maria Fátima Guarizo Klingbeil: Data curation, Review
Virginia Conceição Amaro Martins: Writing - Review & editing, Supervision
Ana Maria de Guzzi Plepis: Writing - Review & editing, Supervision, Project administration.

Declaration of competing interest

The authors declare that they have no known competing financial interests or personal relationships that could have appeared to influence the work reported in this paper.

Acknowledgments

The authors would like to thank the Center of Analytical Chemical Analysis of IQSC/USP, for all the infrastructure available for SEM and EDX analysis. We thank Prof. Dr. Marcia Nitschke (IQSC-USP) by microbiological assays. We also thank Prof. Dr. Monica Beatriz Mathor (Ipen) by sterilization process and cytotoxicity assays.

Appendix A. Supplementary data

Supplementary data to this article can be found online at https://doi.org/10.1016/j.msec.2021.111955.

References

[1] A.J. Ryan, J.P. Gleeson, A. Matsiko, E.M. Thompson, F.J. O'Brien, Effect of different hydroxyapatite incorporation methods on the structural and biological

properties of porous collagen scaffolds for bone repair, J. Anat. 227 (2015) 732–745, https://doi.org/10.1111/joa.12262.
[2] C. Gao, S. Peng, P. Feng, C. Shuai, Bone biomaterials and interactions with stem cells, Bone Res. 5 (2017) 1–33, https://doi.org/10.1038/boneres.2017.59.
[3] X. Liu, C. Zheng, X. Luo, X. Wang, H. Jiang, Recent advances of collagen-based biomaterials: multi-hierarchical structure, modification and biomedical applications, Mater. Sci. Eng. C. 99 (2019) 1509–1522, https://doi.org/10.1016/j.msec.2019.02.070.
[4] J.J. Pearson, N. Gerken, C. Bae, K. Lee, A. Satsangi, S. McBride, M.R. Appleford, D. D. Dean, J.O. Hollinger, J.L. Ong, T. Guda, In vivo hydroxyapatite scaffold performance in infected bone defects, J. Biomed. Mater. Res. Part B Appl. Biomater. 108 (2019) 1–10, https://doi.org/10.1002/jbm.b.34466.
[5] M.M. Stevens, Biomaterials for bone tissue engineering, Mater. Today 11 (2008) 18–25, https://doi.org/10.1016/S1369-7021(08)70086-5.
[6] X. He, X. Fan, W. Feng, Y. Chen, T. Guo, F. Wang, J. Liu, K. Tang, Incorporation of microfibrillated cellulose into collagen-hydroxyapatite scaffold for bone tissue engineering, Int. J. Biol. Macromol. 115 (2018) 385–392, https://doi.org/10.1016/j.ijbiomac.2018.04.085.
[7] S. Minardi, F. Taraballi, F.J. Cabrera, J. Van Eps, X. Wang, S.A. Gazze, J. S. Fernandez-Mourev, A. Tampieri, L. Francis, B.K. Weiner, E. Tasciotti, Biomimetic hydroxyapatite/collagen composite drives bone niche recapitulation in a rabbit orthotopic model, Mater. Today Bio. 2 (2019), 100005, https://doi.org/10.1016/j.mtbio.2019.100005.
[8] M.Á.V. Rodrigues, M.R.V. Bertolo, C.A. Marangon, V.C.A. Martins, A.M.G. Plepis, Chitosan and gelatin materials incorporated with phenolic extracts of grape seed and jabuticaba peel: rheological, physicochemical, antioxidant, antimicrobial and barrier properties, Int. J. Biol. Macromol. 160 (2020) 769–779, https://doi.org/10.1016/j.ijbiomac.2020.05.240.
[9] J.E. Song, J. Tian, Y.J. Kook, M. Thangavelu, J.H. Choi, G. Khang, A BMSCs-laden quercetin/duck's feet collagen/hydroxyapatite sponge for enhanced bone regeneration, J. Biomed. Mater. Res. - Part A. 108 (2020) 784–794, https://doi.org/10.1002/jbm.a.36857.
[10] M.R. Bet, G. Goissis, C.A. Lacerda, Characterization of polyanionic collagen prepared by selective hydrolysis of asparagine and glutamine carboxyamide side chains, Biomacromolecules v.2 (2001) 1074–1079.
[11] G. Goissis, S. Suzigan, D.R. Parreira, J.V. Maniglia, D.M. Braile, S. Raymundo, Preparation and characterization of collagen-elastin matrices from blood vessels intended as small diameter vascular grafts, Artif, Organs. 24 (2000) 217–223.
[12] S. Sarfraz, B. Naseem, S. Amin, M. Mujahid, Synthesis and characterization of nano hydroxyapatite, Adv, Mater. Res. 264–265 (2011) 1370–1375, https://doi.org/10.4028/www.scientific.net/AMR.264-265.1370.
[13] G. Yuan, H. Lv, W. Tang, X. Zhang, H. Sun, Effect of chitosan coating combined with pomegranate peel extract on the quality of Pacific white shrimp during iced storage, Food Control 59 (2016) 818–823, https://doi.org/10.1016/j.foodcont.2015.07.011.
[14] J.B. Lima, A.D. Corrêa, A.A. Saczk, M.P. Martins, R.O. Castilho, Anthocyanins, pigment stability and antioxidant activity in jabuticaba [*Myrciaria cauliflora* (Mart.) O. Berg], Rev. Bras. Frutic. 33 (2011) 877–887, https://doi.org/10.1590/s0100-29452011000300023.
[15] V.L. Singleton, R. Orthofer, R.M. Lamuela-Raventós, Analysis of total phenols and other oxidation substrates and antioxidants by means of Folin-Ciocalteu reagent, Methods Enzymol. 299 (1999) 152–178, https://doi.org/10.1016/S0076-6879(99)99017-1.
[16] A.G.S. Azevedo, K. Strecker, Avaliação da influência da razão Ca/P nos valores de cristalinidade e crescimento de cristalitos durante a sinterização de pós de hidroxiapatita, Eclet. Quim. 39 (2014) 141–150. doi:10.26850/1678-4618eqj.v39.1.2014.p141-150.
[17] International Organization for Standardization, ISO/TS 11137 Sterilization of Health Care Products — Radiation, 2017 (Genebra).
[18] Clinical and Llaboratory Sstandards Iinstitute, CLSI, Methods for Dilution Antimicrobial Susceptibility Tests for Bacteria that Grow Aerobically Approved Standard – 11 Ed. CLSI Document M07-A10, 2018 (Wayne).
[19] Clinical and Llaboratory Sstandards Iinstitute, CLSI, Performance Standards for Antimicrobial Disk Susceptibility Tests – 13 Ed. CLSI Document M02-A12, 2018 (Wayne).
[20] International Organization for Standardization, ISO 10993-12 Biological Evaluation of Medical Devices – Part 12: Sample Preparation and Reference Materials, 2012 (Genebra).
[21] M.A. Nunes, F. Pimentel, A.S.G. Costa, R.C. Alves, M.B.P.P. Oliveira, Cardioprotective properties of grape seed proanthocyanidins: an update, Trends Food Sci, Technol. 57 (2016) 31–39, https://doi.org/10.1016/j.tifs.2016.08.017.
[22] T.K. Patle, K. Shrivas, R. Kurrey, S. Upadhyay, R. Jangde, R. Chauhan, Phytochemical screening and determination of phenolics and flavonoids in Dillenia pentagyna using UV–vis and FTIR spectroscopy, Spectrochim. Acta - Part A Mol, Biomol. Spectrosc. 242 (2020), 118717, https://doi.org/10.1016/j.saa.2020.118717.
[23] D. Ghirardello Agourram, K. Rantsiou, G. Zeppa, S. Belviso, A. Romane, K. Oufdou, M. Giordano, Phenolic content, antioxidant potential, and antimicrobial activities of fruit and vegetable by-product extracts, Int. J. Food Prop. 16 (2013) 1092–1104, https://doi.org/10.1080/10942912.2011.576446.
[24] I.D. Dallabona, G.G. de Lima, B.I. Cestaro, I.S. Tasso, T.S. Paiva, E.J.G. Laureanti, L. M.M. Jorge, B.J.G. da Silva, C.V. Helm, A.L. Mathias, R.M.M. Jorge, Development of alginate beads with encapsulated jabuticaba peel and propolis extracts to achieve a new natural colorant antioxidant additive, Int. J. Biol. Macromol. 163 (2020) 1421–1432.
[25] T. Padrão, C.C. Coelho, P. Costa, N. Alegrete, F.J. Monteiro, S.R. Sousa, Combining local antibiotic delivery with heparinized nanohydroxyapatite/collagen bone substitute: a novel strategy for osteomyelitis treatment, Mater. Sci. Eng. C. 119 (2021) 1–11, https://doi.org/10.1016/j.msec.2020.111329.
[26] O. Hu, Z. Tan, Y. Liu, J. Tao, Y. Cai, M. Zhang, H. Pan, X. Xu, R. Tang, Effect of crystallinity of calcium phosphate nanoparticles on adhesion, proliferation, and differentiation of bone marrow mesenchymal stem cells, J. Mater. Chem. 17 (2007) 4690–4698, https://doi.org/10.1039/B710936A.
[27] M.L.L.R. Menezes, N.R. Pires, P.L.R. da Cunha, M.F. Rosa, B.W.S. Souza, J.P. A. Feitosa, M.S.M. de Souza Filho, Effect of tannic acid as crosslinking agent on fish skin gelatin-silver nanocomposite film, Food Packag, Shelf Life. 19 (2019) 7–15, https://doi.org/10.1016/j.fpsl.2018.11.005.
[28] G. Tripathi, B. Basu, A porous hydroxyapatite scaffold for bone tissue engineering: physico-mechanical and biological evaluations, Ceram. Int. 38 (2012) 341–349, https://doi.org/10.1016/j.ceramint.2011.07.012.
[29] M. Azami, J. Ai, S. Ebrahimi-Barough, M. Farokhi, S.E. Fard, *In vitro* evaluation of biomimetic nanocomposite scaffold using endometrial stem cell derived osteoblast-like cells, Tissue Cell. 45 (2013) 328–337, https://doi.org/10.1016/j.tice.2013.05.002.
[30] S. Alidadi Oryan, A. Moshiri, N. Maffulli, Bone regenerative medicine: classic options, novel strategies, and future directions, J. Orthop. Surg. Res. 9 (2014) 1–27, https://doi.org/10.1186/1749-799X-9-18.
[31] X.R. Zhao, X. Xu, J. Teng, N. Zhou, Z. Zhou, X.Y. Jiang, F.P. Jiao, J.G. Yu, Three-dimensional porous graphene oxide-maize amylopectin composites with controllable pore-sizes and good adsorption-desorption properties: facile fabrication and reutilization, and the adsorption mechanism, Ecotoxicol. Environ. Saf. 176 (2019) 11–19, https://doi.org/10.1016/j.ecoenv.2019.03.069.
[32] C. Mauffrey, D. Seligson, P. Lichte, H.C. Pape, M. Al-Rayyan, Bone graft substitutes for articular support and metaphyseal comminution: what are the options? Injury 42 (2011) S35–S39, https://doi.org/10.1016/j.injury.2011.06.012.
[33] G.H. Billström, A.W. Blom, S. Larsson, A.D. Beswickb, Application of scaffolds for bone regeneration strategies: current trends and future directions, Injury 44 (2013) S28–S33, https://doi.org/10.1016/S0020-1383(13)70007-X.
[34] K. Zhang, Y. Fan, N. Dunne, X. Li, Effect of microporosity on scaffolds for bone tissue engineering, Regen, Biomater. 5 (2018) 115–124, https://doi.org/10.1093/rb/rby001.
[35] V. Karageorgiou, D. Kaplan, Porosity of 3D biomaterial scaffolds and osteogenesis, Biomaterials 26 (2005) 5474–5491, https://doi.org/10.1016/j.biomaterials.2005.02.002.
[36] C.M. Murphy, M.G. Haugh, F.J. O'Brien, The effect of mean pore size on cell attachment, proliferation and migration in collagen-glycosaminoglycan scaffolds for bone tissue engineering, Biomaterials 31 (2010) 461–466, https://doi.org/10.1016/j.biomaterials.2009.09.063.
[37] M.A. Velasco, C.A. Narváez-Tovar, D.A. Garzón-Alvarado, Design, materials, and mechanobiology of biodegradable scaffolds for bone tissue engineering, Biomed Res. Int. 2015 (2015) 1–22. doi:https://doi.org/10.1155/2015/729076.
[38] V. Alt, W.H. Cheung, S.K.H. Chow, U. Thormann, E.N.M. Cheung, K.S. Lips, R. Schnettler, K.S. Leung, Bone formation and degradation behavior of nanocrystaline hydroxyapatite with or without collagen-type 1 in osteoporotic bone defects - an experimental study in osteoporotic goats, Injury 47 (2016) S58–S65, https://doi.org/10.1016/S0020-1383(16)47010-5.
[39] A.C.B.M. Fook, A.H. Aparecida, M.V.L. Fook, Desenvolvimento de biocerâmicas porosas de hidroxiapatita para utilização como scaffolds para regeneração óssea, Rev. Mater. 15 (2010) 392–399, https://doi.org/10.1590/S1517-70762010000300001.
[40] L. Lajnef, I. Caceres, P. Trinsoutrot, F.C. Bouhtoury, N. Ayed, B. Charrier, Effect of *Punica granatum* peel and *Melia azedarach* bark extracts on durability of European beech and maritime pine, Eur. J. Wood Wood Prod. 76 (2018) 1725–1735, https://doi.org/10.1007/s00107-018-1340-x.
[41] T.R. Marques, M.A. Braga, P.H.S. Cesar, S. Marcussi, A.D. Corrêa, Jabuticaba (*Plinia jaboticaba*) skin extracts as inhibitors of phospholipases A2 and proteases, An, Acad. Bras. Cienc. 91 (2019) 1–16, https://doi.org/10.1590/0001-3765201920180248.
[42] D.J. Epasinghe, M.F. Burrow, C.K.Y. Yiu, Effect of proanthocyanidin on ultrastructure and mineralization of dentine collagen, Arch, Oral Biol. 84 (2017) 29–36, https://doi.org/10.1016/j.archoralbio.2017.09.012.
[43] M. Lucarini, F. Sciubba, D. Capitani, M.E. Di Cocco, L. D'Evoli, A. Durazzo, M. Delfini, G.L. Boccia, Role of catechin on collagen type I stability upon oxidation: a NMR approach, Nat. Prod. Res. 34 (2019) 1–10, https://doi.org/10.1080/14786419.2019.1570509.
[44] J. Kozlowska, A. Sionkowska, A.M. Osyczka, M. Dubiel, Stabilizing effect of carbodiimide and dehydrothermal treatment crosslinking on the properties of collagen/hydroxyapatite scaffolds, Polym. Int. 66 (2017) 1164–1172, https://doi.org/10.1002/pi.5371.
[45] Sionkowska, S. Grabska, Preparation and characterization of 3D collagen materials with magnetic properties, Polym. Test. 62 (2017) 382–391, https://doi.org/10.1016/j.polymertesting.2017.07.026.
[46] G. Russmueller, R. Liska, J. Stampfl, C. Heller, A. Mautner, K. Macfelda, B. Kapeller, R. Lieber, A. Haider, K. Mika, C. Schopper, C. Perisanidis, R. Seemann, D. Moser, 3D printable biophotopolymers for *in vivo* bone regeneration, Materials 8 (2015) 3685–3700, https://doi.org/10.3390/ma8063685.
[47] B. Green, X. Yao, A. Ganguly, C. Xu, V. Dusevich, M.P. Walker, Y. Wang, Grape seed proanthocyanidins increase collagen biodegradation resistance in the dentin/adhesive interface when included in an adhesive, J. Dent. 38 (2010) 908–915, https://doi.org/10.1016/j.jdent.2010.08.004.

[48] M. Iafisco Tampieri, M. Sandri, S. Panseri, C. Cunha, S. Sprio, E. Savini, M. Uhlarz, T. Herrmannsdörfer, Magnetic bioinspired hybrid nanostructured collagen-hydroxyapatite scaffolds supporting cell proliferation and tuning regenerative process, ACS Appl. Mater. Interfaces 6 (2014) 15697–15707, https://doi.org/10.1021/am5050967.

[49] R. Bartoszewski Górniak, J. Króliczewski, Comprehensive review of antimicrobial activities of plant flavonoids, Phytochem. Rev. 18 (2019) 241–272, https://doi.org/10.1007/s11101-018-9591-z.

[50] M.C. Silva, V.B. de Souza, M. Thomazini, E.R. da Silva, T. Smaniotto, R.A. de Carvalho, M.I. Genovese, C.S. Favaro-Trindade, Use of the jabuticaba (*Myrciaria cauliflora*) depulping residue to produce a natural pigment powder with functional properties, LWT - Food Sci, Technol. 55 (2014) 203–209, https://doi.org/10.1016/j.lwt.2013.08.026.

[51] D.A. Oliveira, A.A. Salvador, A. Smânia, E.F.A. Smânia, M. Maraschin, S.R. S. Ferreira, Antimicrobial activity and composition profile of grape (*Vitis vinifera*) pomace extracts obtained by supercritical fluids, J. Biotechnol. 164 (2013) 423–432, https://doi.org/10.1016/j.jbiotec.2012.09.014.

[52] B.R. Albuquerque, C. Pereira, R.C. Calhelha, M.J. Alves, R.M.V. Abreu, L. Barrosa, M.B.P.P. Oliveira, I.C.F.R. Ferreira, Jabuticaba residues (*Myrciaria jaboticaba* (Vell.) Berg) are rich sources of valuable compounds with bioactive properties, Food Chem. 309(2020)1–8. doi:https://doi.org/10.1016/j.foodchem.2019.125735.

[53] Klančnik, S. Piskernik, B. Jeršek, S.S. Možina, Evaluation of diffusion and dilution methods to determine the antibacterial activity of plant extracts, J. Microbiol. Methods 81 (2010) 121–126. doi:https://doi.org/10.1016/j.mimet.2010.02.004.

[54] S.C. Wu, Z.Q. Yang, F. Liu, W.J. Peng, S.Q. Qu, Q. Li, X. Bin Song, K. Zhu, J.Z. Shen, Antibacterial effect and mode of action of flavonoids from licorice against methicillin-resistant *Staphylococcus aureus*, Front. Microbiol. 10 (2019) 1–14, https://doi.org/10.3389/fmicb.2019.02489.

[55] C.R. Arciola, D. Campoccia, L. Montanaro, Implant infections: adhesion, biofilm formation and immune evasion, Nat. Rev. Microbiol. 16 (2018) 397–409, https://doi.org/10.1038/s41579-018-0019-y.

[56] N.A. Turner, B.K. Sharma-Kuinkel, S.A. Maskarinec, E.M. Eichenberger, P.P. Shah, M. Carugati, T.L. Holland, V.G. Fowler, Methicillin-resistant *Staphylococcus aureus*: an overview of basic and clinical research, Nat. Rev. Microbiol. 17 (2019) 203–218, https://doi.org/10.1038/s41579-018-0147-4.

[57] C.M.P. Vidal, W. Zhu, S. Manohar, B. Aydin, T.A. Keiderling, P.B. Messersmith, A. K. Bedran-Russo, Collagen-collagen interactions mediated by plant-derived proanthocyanidins: a spectroscopic and atomic force microscopy study, Acta Biomater. 41 (2016) 110–118, https://doi.org/10.1016/j.actbio.2016.05.026.

[58] Z.A.N. Hanani, F.C. Yee, M.A.R. Nor-Khaizura, Effect of pomegranate (*Punica granatum* L.) peel powder on the antioxidant and antimicrobial properties of fish gelatin films as active packaging, Food Hydrocoll. 89 (2019) 253–259, https://doi.org/10.1016/j.foodhyd.2018.10.007.

[59] J.N. Eloff, Avoiding pitfalls in determining antimicrobial activity of plant extracts and publishing the results, BMC Complement, Altern. Med. 19 (2019) 1–8, https://doi.org/10.1186/s12906-019-2519-3.

[60] N. Banerjee, S. Talcott, S. Safe, S.U. Mertens-Talcott, Cytotoxicity of pomegranate polyphenolics in breast cancer cells *in vitro* and *vivo*: potential role of miRNA-27a and miRNA-155 in cell survival and inflammation, Breast Cancer Res, Treat. 136 (2012) 21–34, https://doi.org/10.1007/s10549-012-2224-0.

[61] S. Okonogi, C. Duangrat, S. Anuchpreeda, S. Tachakittirungrod, S. Chowwanapoonpohn, Comparison of antioxidant capacities and cytotoxicities of certain fruit peels, Food Chem. 103 (2007) 839–846, https://doi.org/10.1016/j.foodchem.2006.09.034.

[62] H.D.S. Pitz, A. Pereira, M.B. Blasius, A.P.L. Voytena, R.C.L. Affonso, S. Fanan, A.C. D. Trevisan, R.M. Ribeiro-Do-Valle, M. Maraschin, *In Vitro* evaluation of the antioxidant activity and wound healing properties of Jaboticaba (*Plinia peruviana*) fruit peel hydroalcoholic extract, Oxid. Med. Cell. Longev. 2016 (2016) 1–7. doi: https://doi.org/10.1155/2016/3403586.

[63] C.H. Huang, C.Y. Chi, Y.S. Chen, K.Y. Chen, P.L. Chen, C.H. Yao, Evaluation of proanthocyanidin-crosslinked electrospun gelatin nanofibers for drug delivering system, Mater. Sci. Eng. C. 32 (2012) 2476–2483, https://doi.org/10.1016/j.msec.2012.07.029.